Journal of Applied Polymer Science

Preparation, Characterization, and Performance Evaluation of Coated PES Polymer Materials Fabricated via Dry/Wet Phase Inversion Technique

KeeHong Kim,[1,2] ChanHeui Hyung,[1] Pravin G. Ingole,[1] JongHak Kim,[2] HyungKeun Lee[1]
[1]Korea Institute of Energy Research, 71-2 Jang-dong, Yuseong-gu, Daejeon, Korea
[2]Department of Chemical and Biomolecular Engineering, Yonsei University, Korea
Correspondence to: H. Lee (E-mail: hklee@kier.re.kr).

ABSTRACT: Sulfur dioxide (SO_2) is the major air pollutant which is emitted from the power plant. In this study, hollow fiber membrane (HFM) separation process is applied for the improvement of SO_2 removal efficiency in the post-combustion gas. HFM was produced by dry/wet phase inversion method and then coated with Polydimethylsiloxane (PDMS). The membrane morphology and characterization were examined with help of scanning electron microscope (SEM), energy dispersion of X-ray spectroscopy (EDX), Fourier transform infrared (FT-IR) and atomic force microscopy (AFM). Polyethersulfone (PES) hollow fiber membranes were tested for the SO_2/N_2 binary mixed gas separation. Single gas permeance of SO_2, N_2, and binary mixture gas (200 ppm of SO_2) separation experiment was initiated to observe membrane behavior according to temperature and pressure difference and retentate flow rate. As a result, permeance of SO_2 was 24.9–47.4 GPU and selectivity of SO_2/N_2 was 1.6–4.2. From the mixture gas separation experiment, SO_2 removal efficiency increased according to stage cut and operating pressure. © 2013 Wiley Periodicals, Inc. J. Appl. Polym. Sci. **2014**, *131*, 39711.

KEYWORDS: fibers; membranes; composites; separation techniques; properties and characterization

Received 20 February 2013; accepted 27 June 2013
DOI: 10.1002/app.39711

INTRODUCTION

Combustion of sulfur containing fuels, such as coal, in power plant is the major emission source of sulfur dioxide (SO_2). SO_2 is emitted into atmosphere is main cause of acid rain because it is the most pervasive air pollutant. Moreover, the emission of SO_2 is a major environmental concern because of its hazardous effects on human health and ecosystems.[1,2] At present, limestone–gypsum wet flue gas desulfurization (WFGD) using wet scrubber is the most effective process to control the emission of SO_2. The main task of WFGD system with forced oxidation is elimination of sulfur dioxide from flue gas and production of gypsum as a saleable product.[3]

However, in these days, concentration of SO_2 in the fuel has been increasing because high sulfur fuel usages increased. As a result, the quality of produced gypsum has been decreasing and harmful to the recycle process. Therefore, the emission and concentration of SO_2 will increase because of burning of low-quality coal. Hence, the growing environmental concerns of society have led to more rigorous environmental standard and limits.[4] For example; The U.S. Environmental Protection Agency (EPA) is issuing a new health standard for sulfur dioxide (SO_2). It's been almost 40 years since the SO_2 standards strengthened. Recently, EPA created the new 1-h standard for SO_2, lowering it from 140 ppb to 75 ppb.[5] In addition, Korea ministry of environment controlled daily average standard of SO_2 emission from the power plant, from 150 ppm to 100 ppm.

However, to reach the reinforced standard, exiting system needs the enlargement of process scale or additional FGD system to increase SO_2 removal efficiency. In turn, new upgrading separation technologies have the potential of being more economical than currently used technologies.

For the improvement of SO_2 removal efficiency, the median design was manufactured for the pertinent populations of wet limestone. Particularly, limestone forced oxidation (LSFO) has been increasingly used in the recent past.[6] Recently, membrane gas absorption technology has been researched for acidic gas treatment as alternative to conventional technologies.[7] Luis et al.[8] used the supported ionic liquid membranes (SILMs) for the separation/concentration of SO_2 and CO_2. The SILMs, which was prepared using porous membranes of polyvinylidene fluoride (PVDF) with hydrophilic material and liquid of 1-butylimidaxolium acetate, shows the most promising combination in the researched system. Similarly, Park et al.[9] designed the tree-stages gas–liquid contactor that composed of PVDF

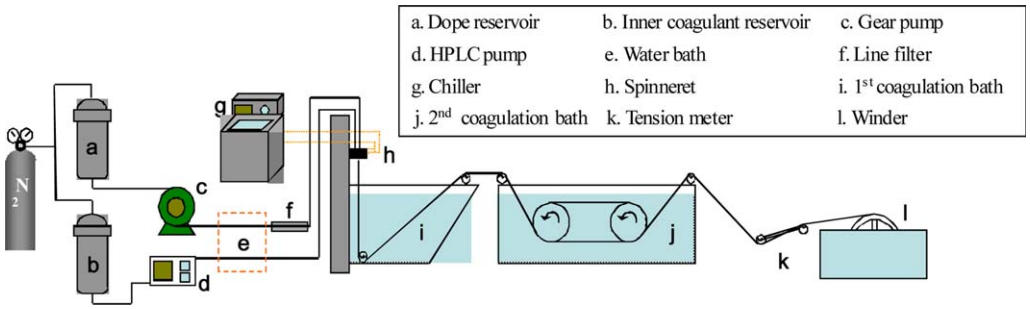

Figure 1. Schematic diagram of HFM spinning system. [Color figure can be viewed in the online issue, which is available at wileyonlinelibrary.com.]

hollow fiber membrane (HFM) and amine adsorbent. Also, Felder et al.[10] researched the permeability, diffusivity, solubility, and activation energies for SO_2 through various polymer membranes. Moreover, Scholes et al.[2] reviewed about separation of minor compound such as SOx, NOx, CO, H_2S, NH_3, in the both pre- and post- combustion use of polymeric membrane process for CO_2 capture. Membrane process has some advantageous over the previous existence methods because of low power usage and costs, simplicity in operation and compactness and portability. It does not need the additive for the separation and easily combines with other process.[11,12]

In this study, polymeric HFM process applied to the additional FGD process for the improvement of SO_2 removal efficiency. For the experiment of the HFM using polyethersulfone (PES), fabricated and prepared the module and was utilized for the removal of SO_2 from mixture gas. PES has excellent thermal and dimensional stability as well as strong chemical resistance. It also has a high degree of chain rigidity because of its regular and polar backbone.[13] Recently, PES hollow fiber membrane has been developed for the oxygen enrichment (O_2/N_2), purification of H_2 and separation of acidic (CO_2, H_2S) gas from natural gases.[14–17] Polydimethylsiloxane (PDMS) was coated on the outer surface of the PES HFM substrate. Additional PDMS coating is only for sealed the defects of the outermost skin of HFM. The coating layer serves to plug defects in the selective layer and reduce the risk of gas permeation. In general, high flux and low selectivity polymer such as PDMS was coated on the fiber.[18,19] For the experiment of single and mixture gas, membrane process was operated at 50–80°C of temperatures and 0.9–1.8 kg_f/cm^2 of pressures.

EXPERIMENTAL

Manufacturing of PES Hollow Fiber Membrane

HFMs were produced by a dry/wet phase inversion method. Commercially available PES (Ultrason® E6020P, BASF, Germany) was used as membrane material. N-methylpyrrolidone (NMP, Merck, Germany) and distilled water were used as the solvent and non-solvent, respectively. Distilled water was used as internal coagulant. HFMs were spun using the set-up schematically shown in Figure 1.

The detailed description of spinning procedures has been elaborated elsewhere.[20] In this study, the air gap—the distance from the spinneret to the first coagulation bath was maintained at 10.0 cm. The composition of the dope solution and spinning condition used in the preparation of the PES HFM are listed in Table I.

Hollow fiber was passed through the first coagulation bath where phase inversion occurred rapidly, and then it moved to the second coagulation bath where it was washed out and coiled around the winder. After this process, the fiber was washed under running water at 40°C for 6 days to remove the remaining solvent. It was then post-treated with methanol for 2 h to improve the flux and dried for 6 days. After drying the outer surface of membrane was coated with PDMS (3.0 wt %) solution. The modules were manufactured with the area of 1.03 m^2 and length of 30 cm for the effectiveness.

Characterization of Membranes

The morphology of PES HFM observed with a scanning electron microscopy (SEM, S-4700, Hitachi) equipped with an energy dispersion of X-ray spectroscopy (EDX, X-max 50, Horiba). The HFM was first freeze-dried with freeze dryer. The dried HFM was slowly cracked in the liquid nitrogen so that a clear cross-sectional fracture is obtained. The fiber was then sputtered by gold using a sputter coating device operated under vacuum. The SEM micrographs for inner surface, outer surface and cross-section of the fiber were taken at various magnifications. EDX analysis was performed in order to investigate the outer surface of HFM. Fourier transform infrared (FT-IR) spectra of substrate and composite membrane were collected by

Table I. Composition of Dope Solution and Spinning Condition for the Preparation of PES HFM

Composition	
PES	27.0 wt %
NMP	68.5 wt %
D.I water	4.5 wt %
Spinning condition	
Air gap	10.0 cm
Spinneret i.d./o.d.	0.12/0.6 mm
Internal coagulant	D.I water
Injection rate of dope solution	3.2 mL/min
Injection rate of internal coagulant	1 mL/min
Winding speed	11 mL/min

Table II. Experimental Conditions for Mixture Gas Separation

Pure gas permeation	
Pressure difference (kg_f/cm^2)	0.9/1.2/1.5/1.8
Temperature (°C)	50/65/80
Mixed gas separation	
Stage cut	0.1/0.3/0.5/0.7
Pressure difference (kg_f/cm^2)	1.2/1.5/1.8
Temperature (°C)	50/65/80
SO_2 concentration in gas mixture	200 ppm

ALPHA-P Spectrometer with a diamond ATR cell (Bruker) in the range of 600–4000 cm^{-1}. Atomic force microscopy (AFM) was used to verification of morphology changes caused by PDMS coating. The values of mean roughness (Ra) values were obtained using a Nanoman AFM system (Veeco) in tapping mode.

Gas Permeation Experiments

The experimental set-up for pure gas permeation and mixed gas separation is shown in Figure 2. For the pure gas permeation experiment, the module was permeated with SO_2 (99.98 vol %, SAFETY GAS, Korea) and N_2 (99.999 vol %, SAFETY GAS, KOREA) with pressure difference of 0.9–1.8 kg_f/cm^2 and temperature of 50–85°C. The permeate side was maintained at atmospheric pressure, and the direction of permeate flow was counter-current for maximum efficiency. Gas permeation rates were measured with a bubble flow meter. Permeance can be described universally by eq. (1)

$$P=\frac{Q}{A\cdot\Delta p} \tag{1}$$

where Q is the gas permeation rate through the membrane, Δp is the gas pressure difference cross the membrane, and A is the effective membrane area. Permeances (P) were expressed in gas permeation unit; GPU was defined as eq. (2)

$$1\,\text{GPU}=1\times10^{-6}\frac{\text{cm}^3(\text{STP})}{\text{cm}^2\cdot\text{cmHg}\cdot\text{sec}} \tag{2}$$

The pure gas selectivity was determined by taking the ratio of the pure gas permeances of i and j components (P_i, P_j):

$$\alpha_{i/j}=P_i/P_j \tag{3}$$

For separation of a gas mixture, a SO_2/N_2 mixture of 200 ppm SO_2 was used. The effect of various operating conditions such as pressure, temperature, and stage cut were tested. All measurements were recorded when the system reached it's a steady state at specific condition. Especially, pressure and stage cut were controlled by retentate control using back pressure regulator. A gas analyzer (A02020, ABB, Germany) was used to detect the composition of the feed, permeate, and retentate stream. The mixed gas was fed to the shell side of the HFM and a vacuum pump was connected to the permeate stream that provided the required vacuum (0.4 kg_f/cm^2). The flow rate and SO_2 concentration of each stream were measured at pressure of 0.9–1.8 kg_f/cm^2, temperature of 50–85°C and stage cut of 0.1–0.7 (Table II).

The stage cut (θ) is can be expressed as eq. (4):

$$\theta=\frac{Q_P}{Q_P+Q_R} \tag{4}$$

where Q_P and Q_R are the permeate and retentate flow rates, respectively.

The separation factor (π) for a binary mixture of components i and j that calculated as eq. (5):

$$\pi=\frac{(C_i/C_j)Permeate}{(C_i/C_j)Feed} \tag{5}$$

where C_i and C_j are the concentrations of each gas in the binary mixture, respectively. The separation factor is the ratio of the compositions of components i and j in the permeate stream relative to the composition ratio of these component in the feed stream. Also, the SO_2 removal efficiency (η) can be calculated by eq. (6)

$$\eta(\%)=\left(1-\frac{C_{i,R}}{C_{i,F}}\right)\times100 \tag{6}$$

where $C_{i,F}$ and $C_{i,R}$ are the concentrations of the i component in the feed and retentate stream, respectively.

RESULTS AND DISCUSSION

Characterization of PES Hollow Fiber Membrane

In this membrane fabrication process an extruded fiber first passes through an air gap where controlled evaporation takes place. Due to the evaporation, the polymer is highly concentrated near the outer surface and a dense membrane top layer is formed. After the air gap the nascent fiber enters a coagulation bath where phase inversion occurs and the membrane structure is arrested. This producer should result in membranes with an asymmetric structure.[21] When the air gap was increased, the selective layer became thicker because of substantial solvent evaporation. Water as a non-solvent additive should exhibit the best miscibility with the coagulant. In addition, water and NMP (solvent) can form a complex through multiple hydrogen bonding. Both the volatile solvent content and the air gap height were found to affect permeation properties. The outer surface

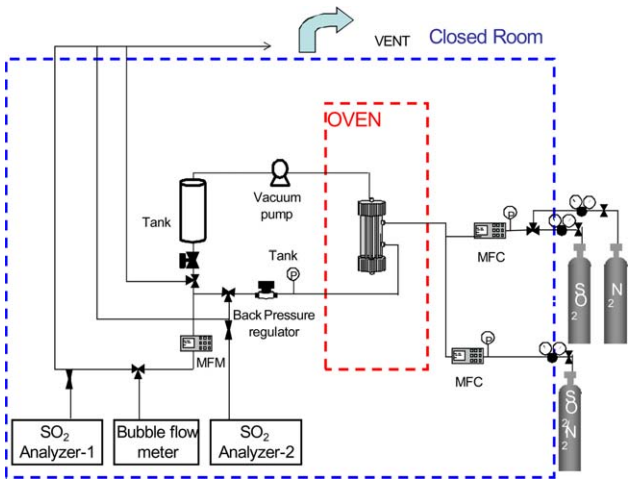

Figure 2. Schematic diagram of the gas permeation apparatus. [Color figure can be viewed in the online issue, which is available at wileyonlinelibrary.com.]

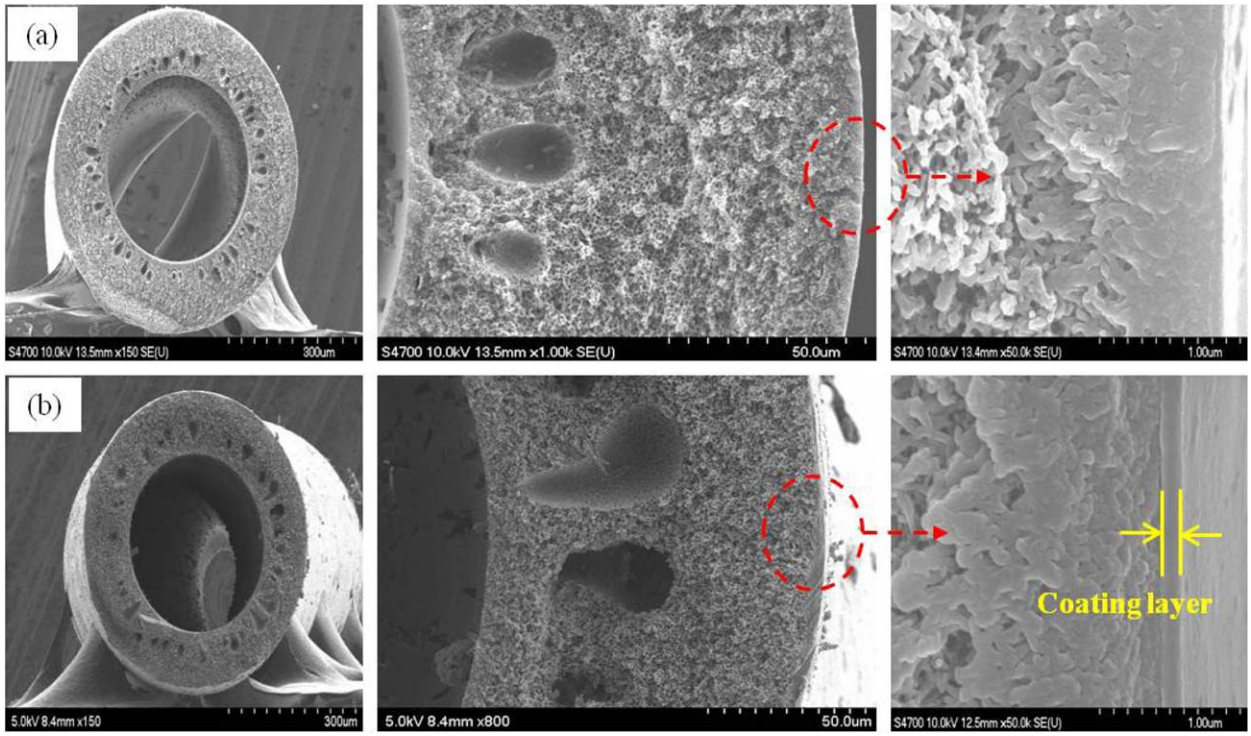

Figure 3. SEM micrograph of cross section of HFM: (a) PES substrate (b) PDMS coated membrane. [Color figure can be viewed in the online issue, which is available at wileyonlinelibrary.com.]

of the fiber with a locally high polymer concentration became thinner as residing time in the air-gap lessoned.[22]

SEM micrographs of the HFM spun from a polymer solution of 27% PES and 68.5% NMP by weight, and coagulated in the pure water bath at the room temperature are shown in Figure 3(a) shows the entire cross section and magnification of the PES HFM. The produced fiber typically has an asymmetric structure; a dense top layer supported by porous, sponge and finger-like substructure. After the coating process, PDMS coating layer (~150 nm) was formed on the outer surface of membrane as shown in Figure 3(b). Apart from the measurable effects of coating on the permeation and selectivity property of the resulting composite membranes formed, a much denser selective layer was observed on the outer surface of coated membrane [Figure 3(b)] as compared to the non-coated membranes [Figure 3(a)].

The top selective layer is clearly seen from the cross-sectional SEM pictures. For the support of characterization we take the EDX analysis of PDMS coated membrane. Figure 4 compared the EDX spectra of outer surface between PES substrate and PDMS coated membrane. As a result, the silicon component was presented on the surface of PES HFM. Figure 4(b) contents

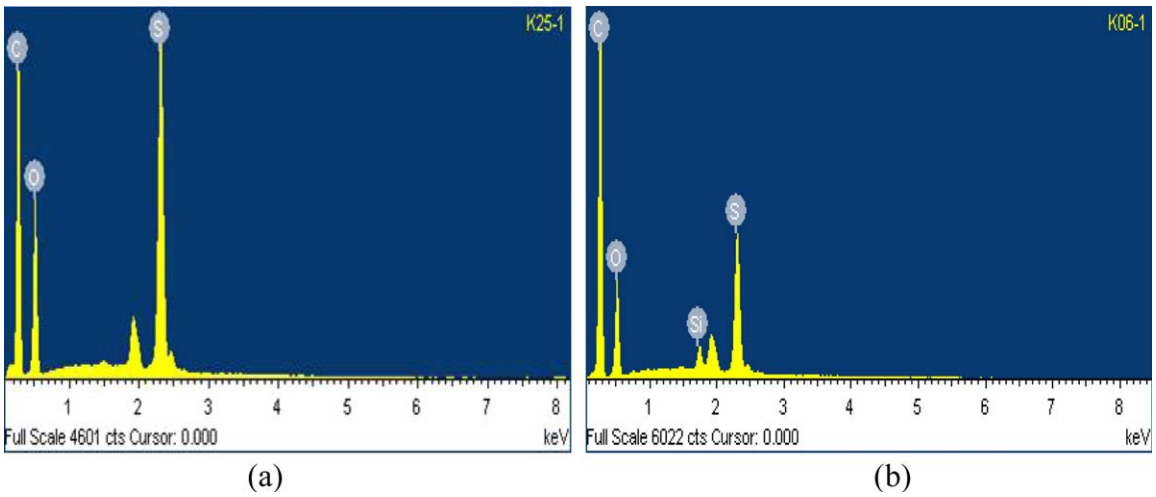

Figure 4. EDX spectra of HFM: (a) PES substrate (b) PDMS coated membrane. [Color figure can be viewed in the online issue, which is available at wileyonlinelibrary.com.]

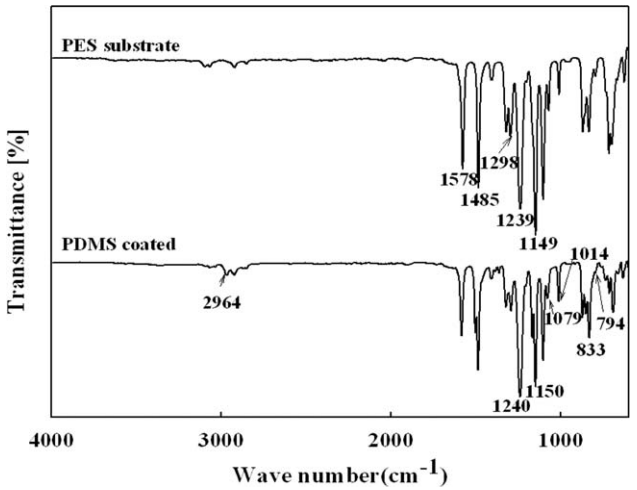

Figure 5. FT-IR spectra of PES substrate and PDMS coated membrane.

the 1.1% (atomic percentage) of Si due to the PDMS coating. It means the coating has been successfully done on the surface of PES hollow fiber support membrane.

Figure 5 presents the FT-IR results for comparison between PES substrate and PDMS coated membrane. PES substrate shows the stretching vibration of sulfone groups appeared at 1149 cm^{-1} and 1298 cm^{-1} are assigned to symmetrical and asymmetrical, respectively. Also, aromatic ether (—C—O—C—) exhibits its characteristic at 1239 cm^{-1}. The peak at 1485 and 1578 cm^{-1} are ascribed to the aromatic benzene rings.[23] As compared with PES substrate, the surface of coated membrane shows CH_3 asymmetric structure at 2964 cm^{-1}, CH_3-Si at 1079 cm^{-1}, Si-O-Si at 1014 cm^{-1}, Si-C at 833 cm^{-1}, and S-$(CH_3)_2$ at 794 cm^{-1}, respectively. These are characteristic peaks of PDMS.[24,25]

Figure 6 shows the typical AFM images of the surface topography before and after coating with PDMS solution. In comparison with Figure 5(a,b), significant changes in surface morphology were observed. The surface of PDMS/PES HFM was much rougher than that of PES support membrane. The values of mean roughness (Ra), which were obtained based on 3.0 × 3.0 μm scan area [Figure 5(a,b)], increased from 2.572 to 10.422 nm. The increase of Ra might be attributed to the surface enrichment of PDMS. The roughness of the membrane indicates difference between valley and ridge impressions in the morphology of the membrane.

Pure Gas Permeance of SO_2 and N_2

Figure 7 presents the effects of PDMS coating on the PES HFM to gas performance. Nascent fiber shows the high permeance and low selectivity ($SO_2/N_2 \approx 0.9$) because of defects and pinholes on the fiber. After the coating on the fiber, gas transport through the membrane take place solution-diffusion process. The solution-diffusion mechanism in polymeric membrane can be defined using Fick's first law according to eq. (7).

$$P = S.D \tag{7}$$

where P is the permeability, D is the diffusivity and S is the solubility. Solubility is a thermodynamic parameter and gives a measure of the amount of penetrant sorbed by the membrane under equilibrium conditions.[26] Solubility is more influenced by operating pressure than diffusion coefficient. As a result, the SO_2 permeance the SO_2/N_2 selectivity highly increased with pressure.

Figure 8(a,b) presents the permeance and selectivity according to increasing operating pressure and temperature. The permeance of SO_2 increased from 38.8 GPU to 47.4 with increasing gas pressure at 50°C, whereas permeance of N_2 was essentially independent from pressure.

From the results of temperature experiment, permeance of SO_2 decreased from 47.4 GPU to 34.1 GPU but oppositely, N_2 increased from 11.4 GPU to 15.2 GPU. This result compared to other polymeric membrane as shown in Table III. The SO_2/N_2 selectivity of PES HFM shows lower than other results due to the operating condition (lower pressure, higher temperature). Especially, operating temperature significantly affect to permeance of SO_2 and N_2. The relationship between gas permeance

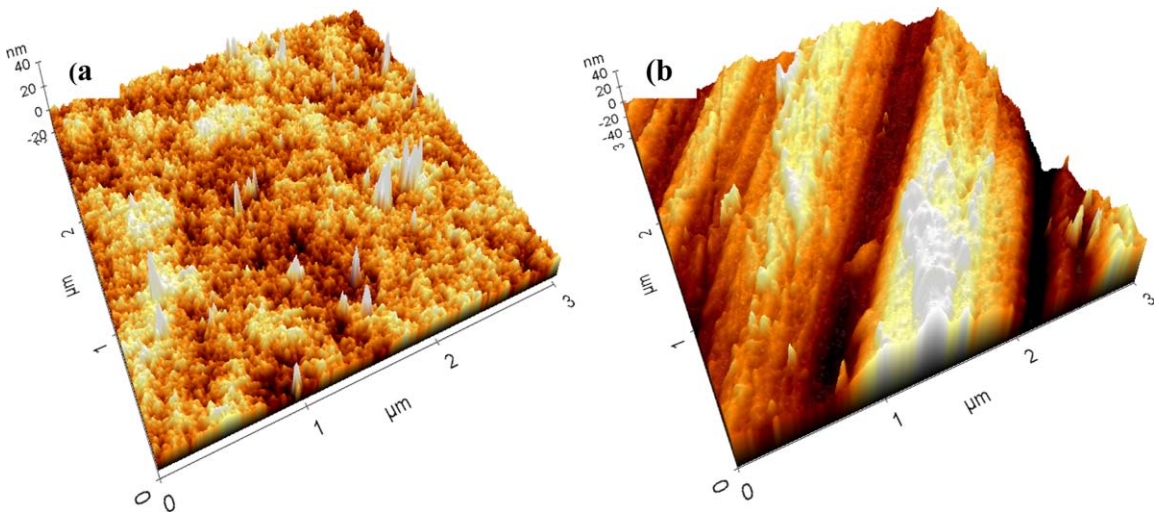

Figure 6. AFM images of PES substrate and PDMS coated membrane. [Color figure can be viewed in the online issue, which is available at wileyonlinelibrary.com.]

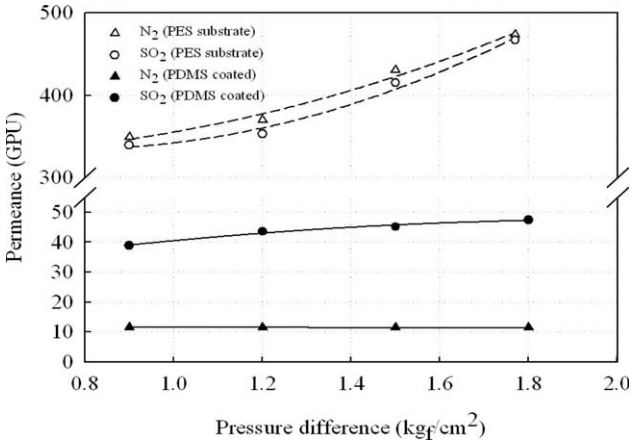

Figure 7. Comparison of gas permeance performance between PES substrate and PDMS coated membrane.

and temperature can be described by van't Hoff-Arrhrenous equation.[29]

$$P = P_0 \exp\left(-\frac{E_P}{RT}\right) \tag{8}$$

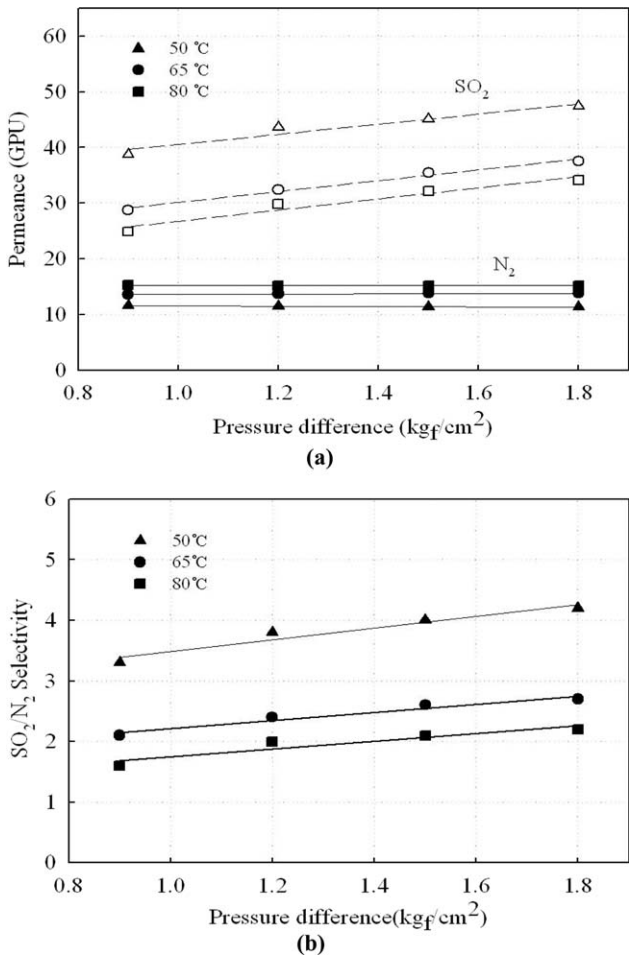

Figure 8. Pure gas permeance of SO_2, N_2 depending on the pressure difference and temperature: (a) permeance and (b) selectivity.

Table III. Comparison of the Separation Performance with Other Polymeric Membranes

Membrane	Pressure difference (kg_f/cm^2)	Operating temperature (°C)	SO_2/N_2 selectivity	Reference
Polycarbonate-K	2.4	22	16.9	27
PVTMS	2.4	22	10.9	27
CTA/PA	1.0	25	14.2	28
This study	1.8	50	4.2	-

P_0 denotes a pre-exponential factor and E_P is the activation energy for permeation. The activation energy for permeation is comprised of the activation energy for diffusion and the heat of sorption:

$$\Delta E_P = \Delta E_D + \Delta H_S \tag{9}$$

where E_D expressed the activation energy for diffusion and ΔH_S is the heat of sorption. Similarly, a temperature effect can be observed for the diffusion of gases in a polymer. Diffusion always increases with increasing temperature; that is, the energy of activation for diffusion is positive ($\Delta E_D > 0$). *S*, on the other hand, increases with decreasing temperature; that is, the heat of solution is negative ($\Delta H_S < 0$).[30]

Figure 9 shows an Arrhenius plot of SO_2 and N_2 from the temperature increasing experiment. SO_2 is a condensable gas that has high critical temperature (430.6 K) and pressure (77.7 bar). As a result, SO_2 is negative activation energy (−10.5 kJ/mol·K) that means permeance strong influence from solubility. However, activation energy of N_2 was 9.13 kJ/mol·K because of a permeance related with diffusivity. Free volume of polymeric membrane was affected by the inherent condensability of penetrant. Condensation occurred by the increase of pressure, increased gas diffusivity and thus permeance increased.[21] However, solubility was decreased according to temperature increase. As a result, compared with permeance of non-condensable gas, permeance of SO_2 was decreased. In the polymeric membranes, the gas permeation is described by the solubility of specific gases within the membrane and their diffusion through the dense polymer matrix. Hence, separation is not just diffusion

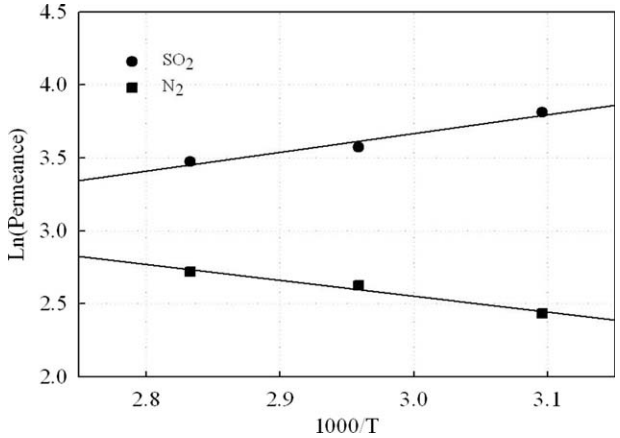

Figure 9. Arrhenius plot of SO_2, N_2 at ΔP = 1.8 kg_f/cm^2.

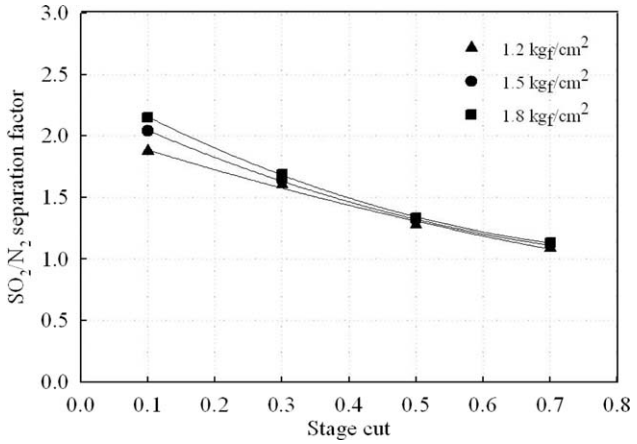

Figure 10. Separation factor depending on the pressure and stage cut at 50°C.

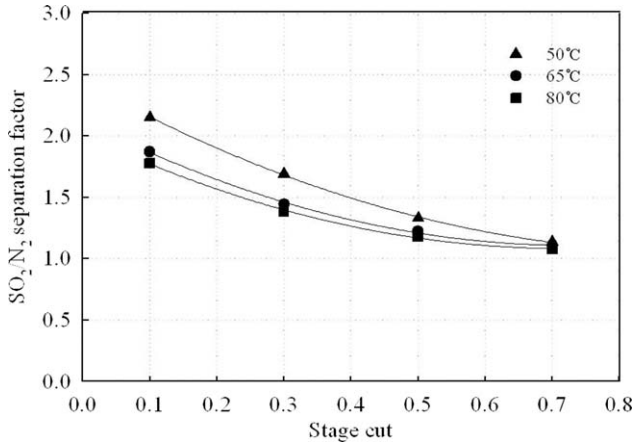

Figure 12. Separation factor according to depending on the temperature and stage cut at 1.8 kg_f/cm^2.

dependent but also reliant on the physical–chemical interaction between the gases and the polymer.[31]

SO_2/N_2 Mixed Gas Separation

Effect of Pressure Difference. 200 ppm of SO_2 and N_2 balanced mixture was prepared for the estimation of SO_2 removal efficiency according to operating conditions. Figure 8 presents a change of the separation factor according to pressure and stage cut at 50°C. Separation factor decreased according to the pressure increase. Separation factor is defined as the variableness of gas concentration between the feed and permeate stream which was permeated species faster than others in the mixed gas, which is the SO_2 in this experiment.[32] As a result of a single gas permeance experiment, SO_2 permeance was strongly affected by the increase of pressure, but N_2 permeance was not. Therefore, separation factor increased with increasing pressure as shown in Figure 10.

Figure 11 demonstrates the tendency of SO_2 removal efficiency and concentration in the retentate stream depending on the operating pressure and stage cut at 50°C. SO_2 removal efficiency was increased with increasing stage cut. The increase of stage cut indicates that the permeate flow rate increased at a constant operating pressure. As a result, it generates coercive permeation, and all of the species in the mixture gas are thereby easily permeated. Therefore, the concentration of N_2 in permeate stream increased relative to that of SO_2. Therefore, N_2 permeation increased while the permeation flow rate increased, because the separation factor increased with stage cut increase. In Figure 9, SO_2 removal efficiency also verified differently with pressure difference. On the contrary to this, SO_2 removal efficiency was decreased at the higher stage cut (>0.5). Removal efficiency can be defined as the difference of SO_2 concentration between the permeate stream and the feed stream. Therefore, accelerated permeation flux was occurred by the increased driving force. The permeation of SO_2 is more preferentially permeate to maximum driving force. In contrast, N_2 permeation was increased consistently with its increasing pressure. As a result, SO_2 removal efficiency was decrease according to pressure increase at higher stage cut (>0.5).

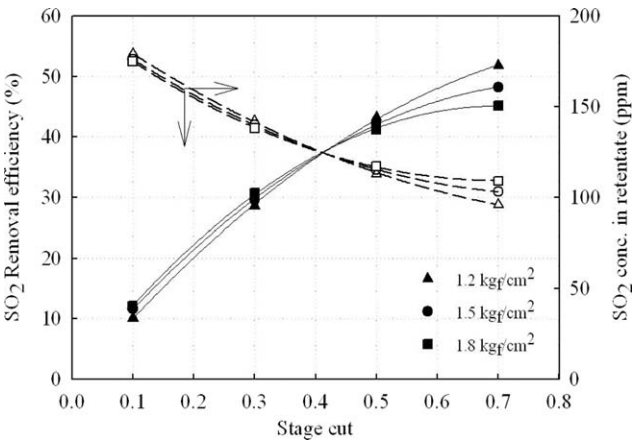

Figure 11. SO_2 removal efficiency and concentration in retentate stream depending on the pressure and stage cut at 50°C.

One of the factors is concentration polarization. Concentration polarization means that a concentration gradient is building up due to depletion of the more permeable component and accumulation of the less permeable species in the boundary layer adjacent to the membrane.[33] Also, N_2 has large portioned in the mixed gas. As a result, SO_2 permeation was disrupted by concentration polarization of N_2 gas in the mixture. Then, concentration of SO_2 in the permeate stream was decreased and then, removal efficiency was decreased at higher pressure.

Effect of Temperature Difference. For the confirmation of temperature effects, the concentration and flow rate in the feed and retentate stream were measured, respectively, at the 1.8 kg_f/cm^2 of operating pressure. From the result of single gas permeance experiment, permeance of SO_2 decreased with increasing temperature because the SO_2 permeability was strongly influenced by the solution coefficient.[27] On the other hand, the permeance of N_2 increased in permeate stream because it was related with diffusion coefficient. Therefore,

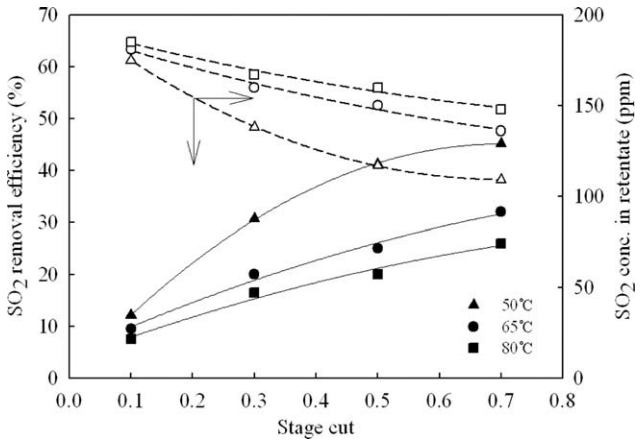

Figure 13. SO_2 removal efficiency and concentration in retentate stream depending on the temperature and stage cut at 1.8 kg_f/cm^2.

separation factor decreased with increasing the temperature, as shown in Figure 12.

Figure 13 shows the change of SO_2 removal efficiency and concentration in the retentate stream while the temperature increased from 50°C to 85°C. SO_2 removal efficiency decreased with temperature increase. Especially, SO_2 removal efficiency was decreased rapidly between 50°C and 65°C, which also correspond with the decrease of SO_2/N_2 selectivity. Therefore, low selectivity influenced SO_2 concentration to decrease in the permeate stream. As a result, the SO_2 concentration in the retentate stream increased with increasing the operating temperature.

CONCLUSION

In this study, the PES HFM was produced by dry/wet phase inversion method. Fabricated membrane shows the asymmetric structure that is composed of dense top layer and porous substrate. The morphology of substrate was characterized by using SEM and EDX. FTIR and AFM examined to compare between PES substrate and PDMS coated membrane. The SEM images clearly demonstrated that an integrated selective layer was formed it also confirmed from EDX results. The AFM analysis showed that the composite membrane surface became much rougher after coating of PDMS.

Pure gas of SO_2 and N_2 were tested for the calculation of single gas permeance. As a result, permeance of SO_2 was increased in the operating pressure while that of N_2 was essentially independent from pressure change. However, selectivity decreased with increasing temperature because they have different permeation mechanisms. Permeance of SO_2 was affected by solubility but N_2 was dominated by diffusivity. This can be evaluated from Arrhenius equation.

200 ppm of SO_2 and N_2 balanced mixture gas was used for the separation test in terms of the operating pressure, temperature and stage cut. SO_2 removal efficiency was increased according to stage cut and pressure increase. However, similar to the result of SO_2/N_2 selectivity, SO_2 removal efficiency decreased with temperature increase. Therefore, concentration of SO_2 in the emitted gas can be decreased to less than 100 ppm according to operating condition control by using polymeric membrane.

ACKNOWLEDGMENT

This work was supported by the Energy Efficiency of the Korea Institute of Energy Technology Evaluation and Planning (KETEP) grant funded by the Korea government Ministry of Knowledge Economy (No. 2011T100100197).

REFERENCES

1. Lee, H. K.; Jo, H. D.; CHoi, W. K.; Park, H. H.; Lim, C. W.; Lee, Y. T. *Desalination* **2006**, *200*, 604.
2. Scholes, C. A.; Kentish, S. E.; Stevens, G. W.; *Sep. Purif. Rev.* **2009**, *38*, 1.
3. Zhong, Y.; Gao, X.; Huo, W.; Luo, Z. Y.; Ni, M. J.; Cen, K. F. *Fuel Process. Technol.* **2008**, *89*, 1025.
4. Cristóbla, J.; Guillén-Gosálbez, G.; Jiménez, L.; Irabien, A. *Appl. Ener.* **2012**, *92*, 369.
5. Environmental Protection Agency. Available at: < http://www.epa.gov/air/sulfurdioxide/>
6. Srivastava, R. K.; Jozewicz, W.; Singer, C. *Environ. Prog.* **2012**, *20*, 219.
7. Lu, Y.; Yu, X.; Tu, S. T.; Yan, J.; Dahlquist, E. *Appl. Ener.* **2012**, *97*, 283.
8. Luis, P.; Neves, L. A.; Afonso, C. A. M.; Coelhoso, I. M.; Crespo, J. G.; Garea, A.; Irabien, A. *Desalination* **2009**, *245*, 485.
9. Park, H. H.; Deshwal, B. R.; Kim, I. W.; Lee, H. K. *J. Membr. Sci.* **2008**, *319*, 29.
10. Felder, R. M.; Spence, R. D.; Ferrell, J. K. *J. Chem. Eng. Data* **1975**, *20*, 235.
11. Hao, J.; Rice, P. A. *J. Membr. Sci.* **2008**, *320*, 108.
12. David, O. C.; Gorri, D.; Urtiaga, A.; Oriz, I. *J. Membr. Sci.* **2011**, *378*, 359.
13. Wang, D.; Li, K.; Teo, W. K. *J. Membr. Sci.* **1996**, *115*, 85.
14. Chen, Y.; Miyano, T.; Fouda, A.; Matsuura, T. *J. Membr. Sci.* **1990**, *48*, 203.
15. Ismail, A. F.; Lorna, W. *Sep. Purif. Technol.* **2002**, *27*, 173.
16. Wang, D.; Li, K.; Teo, W. K. *J. Membr. Sci.* **2000**, *176*, 147.
17. Qin, J. J.; Chung, T. S. *J. Membr. Sci.* **2004**, *229*, 1.
18. Zhang, L.; He, G.; Zhao, W.; Nie, F.; Li, X.; Tan, M. *J. Membr. Sci.* **2011**, *371*, 141.
19. Wang, D.; Li, K.; Teo, W. K. *J. Membr. Sci.* **1998**, *138*, 193.
20. Kim, K. H.; Baik, K. J.; Kim, I. W.; Lee, H. K. *Sep. Sci. Technol.* **2012**, *47*, 963.
21. Xu, Z. L.; Qusay, F. A. *J. Membr. Sci.* **2004**, *223*, 101.
22. Fu, Y. J.; Hu, C. E.; Lee, K. R.; Tsai, H. A.; Ruaan, R. C.; Lai, J. Y. *Eur. Polym. J.* **2007**, *43*, 959.
23. Saedi, Sh.; Madaeni, S. S.; Arabi Shamsabadi, A.; Mottaghi, F. *Sep. Purif. Technol.* **2012**, *99*, 104.
24. Hsu, F. Y.; Kuo, K. L.; Liou, H. M. *J. Taiwan Inst. Chem. E.* **2012**, *43*, 165.

25. Hemmilä, S.; Cauich-Rodríguez, J. V.; Kreutzer, J.; Kallio, P. *Appl. Surf. Sci.* **2012**, *258*, 9864.

26. Mulder, M., Basic Principles of Membrane Technology, 2nd ed.; Kluwer Academic Publishers: Dordrecht, Netherlands, **1996**.

27. Dytnerskii, Y. I.; Karamanov, G. G.; Storzhuk, I. P.; Kovalenko, N. F. *J. Membr. Sci.* **1989**, *41*, 49.

28. Kuehne, D. L.; Friendlander, S. K. *Ind. Eng. Chem. Process Des. Dev.* **1980**, *19*, 616.

29. Ren, X.; Ren, J.; Li, H.; Feng, S.; Deng, M. *Int. J. Greenh. Gas Con.* **2012**, *8*, 111.

30. Wilks, B.; Rezac, M. E. *J. Appl. Polym. Sci.* **2002**, *85*, 2436.

31. Kim, D. H.; Kim, G. L.; Jo, H. D.; Park, J. S.; Lee, H. K. *Korean Chem. Eng. Res.* **2010**, *48*, 660.

32. Peer, M.; Kmali, S.M.; Mahdeyarfar, M.; Mohammadi, T. *Chem. Eng. Technol.* **2007**, *30*, 1418.

33. Deshmukh, S. P.; Li, K. *J. Membr. Sci.* **1998**, *150*, 75.